Shear-induced solidification of athermal systems with weak attraction

Wen Zheng, Hao Liu, and Ning Xu*

CAS Key Laboratory of Soft Matter Chemistry, Hefei National Laboratory for Physical Sciences at the Microscale, and Department of Physics, University of Science and Technology of China, Hefei 230026, People's Republic of China

(Received 14 March 2016; revised manuscript received 26 November 2016; published 19 December 2016)

We find that unjammed packings of frictionless particles with rather weak attraction can always be driven into solidlike states by shear. The structure of shear-driven solids evolves continuously with packing fraction from gel-like to jamminglike, but is almost independent of the shear stress. In contrast, both the density of vibrational states (DOVS) and force network evolve progressively with the shear stress. There exists a packing fraction independent shear stress σ_c, at which the shear-driven solids are isostatic and have a flattened DOVS. Solidlike states induced by a shear stress greater than σ_c possess properties of marginally jammed solids and are thus strictly defined shear jammed states. Below σ_c, shear-driven solids with rather different structures are all under isostaticity and share common features in the DOVS and force network. Our study leads to a jamming phase diagram for weakly attractive particles, which reveals the significance of the shear stress in determining properties of shear-driven solids and the connections and distinctions between jamminglike and gel-like states.

DOI: 10.1103/PhysRevE.94.062608

I. INTRODUCTION

Particulate systems such as colloids, emulsions, foams, and granular materials can form disordered solids at high packing fractions [1–11]. The critical packing fraction of the transition from liquidlike to solidlike states is sensitive to the interaction [11–13] and geometry [14–17] of particles. Consider the simplest case of static packings of spheres. If the spheres are frictionless and purely repulsive, the transition happens as the jamming transition at a critical packing fraction ϕ_j [5,18–22]. The jamming transition is signaled by the sudden formation of a rigid and isostatic force network, i.e., the average coordination number is equal to twice the dimension of space. The physics of jamming is of great importance and broad interest in understanding various transitions from liquidlike to solidlike states for various materials and the nature of amorphous solids.

Over the past two decades, the jamming transition has been almost exclusively studied for purely repulsive particles. Our knowledge about the jamming of attractive particles remains rather poor over a surprisingly long time, while such knowledge is important in practice because many real systems unavoidably contain cohesive particles. Up to date, what we can learn about the jamming of attractive particles may be still from an early experimental study [3]. That work shows expectable results that the presence of attraction smears out ϕ_j, so that a nonvanishing yield stress or glass transition temperature extends to low packing fractions. However, there are in-depth questions that ought to be but have not yet been attacked. For instance, in the zero attraction limit, will attraction simply act as a perturbation and hence just quantitatively extend the jamming phase diagram of purely repulsive particles or lead to qualitatively different phenomena? Moreover, in the presence of attraction, gels are formed at low packing fractions and evolve into glasses or jamminglike states at high packing fractions [7–10,12]. This at least implies that there are distinct regimes in the "jammed" region of the jamming phase diagram for attractive particles [3] that should be partitioned, and the roles of packing fraction, shear stress, and temperature in identifying various solidlike states need to be carefully figured out.

Here we attack the above questions by investigating how attraction affects the picture of jamming established for purely repulsive systems [5] at zero temperature ($T = 0$) and finite shear stresses. We study the formation and properties of shear-driven solids of particles interacting via a repulsive core and a tiny attractive tail. By applying quasistatic shear, we can always find solidlike states below the jamming transition, where the probability of finding solidlike states is almost zero in the absence of shear. By minimizing a thermodynamiclike potential [23,24], we sample solidlike states at fixed packing fraction ϕ and shear stress σ, and analyze their structure, force network, and vibrational properties. The analysis enables us to construct a jamming phase diagram in the σ-ϕ plane at $T = 0$. In particular, there is a packing fraction independent shear stress σ_c. When $\sigma = \sigma_c$, shear-driven solids exhibit features of marginally jammed solids, e.g., being isostatic and having a flattened density of vibrational states (DOVS) [5,25–27]. Solidlike states driven by $\sigma > \sigma_c$ are thus strictly defined shear jammed states.

II. MODEL AND METHODS

To avoid crystallization, we put $N/2$ large and $N/2$ small spherical particles with equal mass m into a box with side length L in all directions. The diameter ratio of the large to small particles is 1.4. The interparticle potential is [12,28]

$$U(r_{ij}) = \begin{cases} \frac{\epsilon}{\alpha}\left(\left|1-\frac{r_{ij}}{d_{ij}}\right|^{\alpha} - 2\mu^{\alpha}\right), & \frac{r_{ij}}{d_{ij}} \leqslant 1+\mu, \\ -\frac{\epsilon}{\alpha}\left(1+2\mu-\frac{r_{ij}}{d_{ij}}\right)^{\alpha}, & 1+\mu < \frac{r_{ij}}{d_{ij}} \leqslant 1+2\mu, \\ 0, & \frac{r_{ij}}{d_{ij}} > 1+2\mu, \end{cases} \tag{1}$$

where r_{ij} and d_{ij} are the separation between particles i and j and sum of their radii, and μ is a tunable parameter to control the range and strength of attraction. We study both harmonic ($\alpha = 2$) and Hertzian ($\alpha = 5/2$) systems. We set the units of

*ningxu@ustc.edu.cn

mass, energy, and length to be particle mass m, characteristic energy scale of the potential ϵ, and small particle diameter d_s.

The shear deformation is realized by introducing the shear strain γ and applying the Lees-Edwards boundary conditions [29]. Without shear ($\gamma = 0$), we generate static states at fixed packing fraction by applying the fast inertial relaxation engine (FIRE) method [30] to minimize the potential energy $U = \sum_{ij} U(r_{ij})$ of random configurations, where the sum is over all pairs of particles. To perform quasistatic shear, we successively increase the shear strain γ by a step strain $\Delta\gamma$, followed by the minimization of U. To well control the shear stress σ, we instead minimize a thermodynamiclike potential $H = U - \sigma\gamma L^d$ [24], where d is the dimension of space. During the minimization, σ is fixed, while γ becomes a variable.

The structure of the system is characterized by the static structure factor $S(q) = \langle|\sum_j \exp(i\vec{q}\cdot\vec{r}_j)|^2\rangle/N$, where $q = |\vec{q}|$ is the angular wave number, $\vec{r}_j$ is the location of particle j, $\langle.\rangle$ denotes the average over states, and the sum is over all particles. The normal modes of vibration are obtained from diagonalizing the Hessian matrix using ARPACK [31]. The DOVS is then calculated as $D(\omega) = \langle\sum_l \delta(\omega - \omega_l)\rangle/dN$, where ω_l is the frequency of the lth normal mode of vibration, $\langle.\rangle$ denotes the average over configurations, and the sum is over all modes.

III. RESULTS

In this work, we are mainly concerned about the solidification in the $\sigma - \phi$ plane at $T = 0$. If not specified, results are shown for $N = 1024$ harmonic systems in two dimensions. We will also show (and specify) results of system size effects, Hertzian systems, and three-dimensional harmonic systems to generalize our major findings.

A. Shear-induced solidification

We vary the strength of attraction μ from 10^{-2} to 10^{-6}, approaching the zero attraction limit. Figure 1(a) shows the probability $P_0(\phi)$ of finding solidlike states for different values of μ by quickly minimizing the potential energy of 10 000 random states without shear. With increasing μ, $P_0(\phi)$ shifts to lower packing fractions. Employing the definition in early work [5], we determine the jamming transition threshold $\phi_{j,\mu}$ from $P_0(\phi)$. As shown in Fig. 1(b), $\phi_j - \phi_{j,\mu} \sim \mu^{1/3}$ in the small μ limit, where $\phi_j \approx 0.842$. Without shear, the attraction seems to play the role of a perturbation.

Figure 1(a) indicates that well below $\phi_{j,\mu}$, by the direct-quench sampling without shear, it is almost impossible to find solidlike states. Starting from unjammed states, we apply quasistatic shear. As shown in Fig. 1(c), in the early stage of the quasistatic shear, the system remains unjammed ($\sigma = 0$). Interestingly, as long as the step strain $\Delta\gamma$ is small enough, nonzero shear stress emerges and fluctuates when $\gamma > \gamma_c$, signaling the formation of solidlike states. The solid forming ability under quasistatic shear decreases when packing fraction decreases, demonstrated by the growth of $\langle\gamma_c\rangle$ in Fig. 1(d), where $\langle.\rangle$ denotes the average over independent runs of quasistatic shear.

A similar phenomenon called shear jamming has also been observed in packings of frictional particles [11]. For frictional

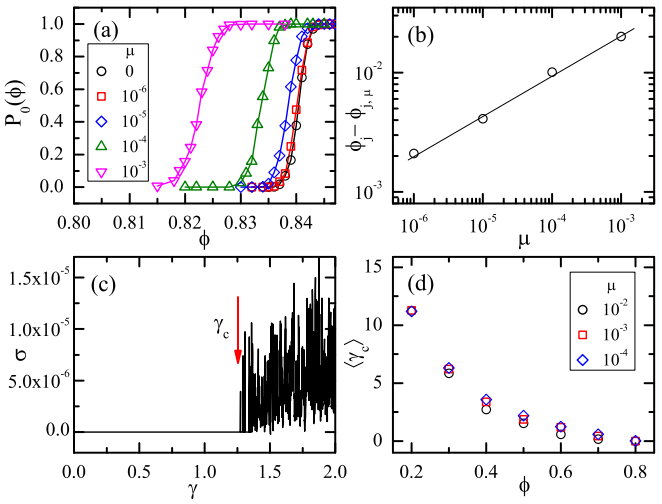

FIG. 1. (a) Probability of finding jammed states without shear, $P_0(\phi)$, for different strength of attraction μ. The lines are a guide for the eye. (b) Critical scaling of the jamming transition threshold: $\phi_j - \phi_{j,\mu} \sim \mu^{1/3}$, with the line having a slope of 1/3. (c) Stress-strain relation of an initially unjammed state at $\phi = 0.60$ and $\mu = 10^{-3}$ under quasistatic shear. The arrow points to the onset shear strain γ_c at which solidlike states start to be explored. (d) Packing fraction dependence of $\langle\gamma_c\rangle$ for different μ.

particles, jamming can happen at packing fractions lower than ϕ_j [13,32], where both jammed and unjammed states exist. Consequently, originally unjammed packings of frictional spheres can jam under quasistatic shear [11]. The underlying physics of such a shear jamming phenomenon still remains elusive and is a hot topic in the field of granular materials [33,34]. In comparison, the shear-induced solidification of attractive particles illustrated in Fig. 1 may convey richer and more complicated physics, at least because of the possible existence of various types of solidlike states. Furthermore, attraction and friction are intrinsically distinct in stabilizing particles. It is interesting to know how attractive particles behave under shear and whether their behaviors could also shed some light on our understanding of shear jamming of frictional particles.

B. Yield stress

During quasistatic shear, the shear stress fluctuates and is not controllable, as shown in Fig. 1(c). To have a clear picture of the shear stress dependence (which turns out to be important), we instead sample shear-driven solids by a recently developed algorithm [23,24] to well control the shear stress. By minimizing a thermodynamiclike potential H of random states, as introduced in Sec. II, we can quickly look for solidlike states at desired shear stress. As shown in Fig. 1, it takes some shear strain to find shear-driven solids. Furthermore, it is impractical to let $\gamma \to \infty$. We thus set a maximum strain $\gamma_m = 20$. The search for shear-driven solids fails once $\gamma > \gamma_m$.

For each pair of ϕ and σ, we run 1000 independent trials and calculate the probability of finding solidlike states $P(\sigma,\phi)$, as shown in Fig. 2(a). At fixed ϕ, $P(\sigma) \approx 1$ when σ is small. For finite size systems, $P(\sigma)$ decreases with increasing σ near the yield stress σ_y [23,24,35], which we determine from

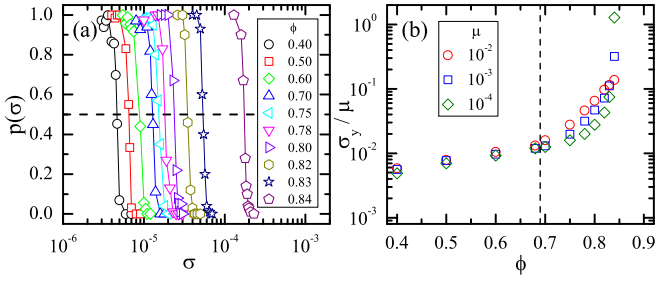

FIG. 2. (a) Probability of finding solidlike states under applied shear stress σ, $P(\sigma)$, at various packing fractions ϕ for $\mu = 10^{-3}$. The horizontal dashed line labels $P(\sigma) = 0.5$. It intersects each $P(\sigma)$ curve at σ_y, defined as the yield stress. The solid lines are a guide for the eye. (b) Yield stress curves $\sigma_y(\phi)$ scaled by the strength of attraction μ. The vertical dashed line labels $\phi = \phi_{rp}$.

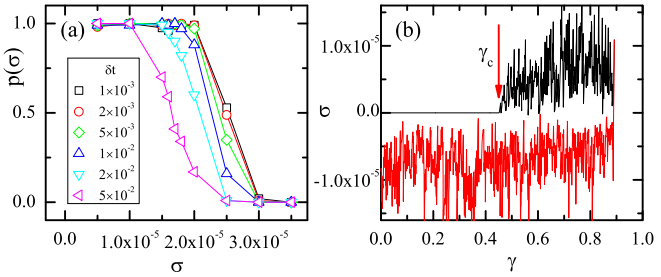

FIG. 3. (a) Evolution of probability of finding shear-driven solids $P(\sigma)$ with the initial input value of "time step" δt required by the FIRE method, for systems at $\phi = 0.80$ ($\mu = 10^{-3}$). The lines are a guide for the eye. (b) Shear strain γ evolution of the shear stress σ under quasistatic shear of a system at $\phi = 0.70$ ($\mu = 10^{-3}$). The initial state at $\gamma = 0$ is unjammed. Shear-driven solids are formed after $\gamma = \gamma_c$ (black curve), as pointed by the arrow. The system is sheared backwards to $\gamma = 0$ (red curve) after γ reaches 0.9. The inverse direction of the shear leads to negative values of the shear stress.

$P(\sigma_y) = 0.5$. Figure 2(b) shows $\sigma_y(\phi)$ for different strength of attraction μ. σ_y decreases with decreasing ϕ, and remains nonzero down to rather low packing fractions. At fixed ϕ, σ_y decreases when μ decreases. Interestingly, roughly below the rigidity percolation threshold at $\phi_{rp} \approx 0.689$ [12], $\sigma_y \sim \mu$, while it breaks down when $\phi > \phi_{rp}$. We will see later that ϕ_{rp} does not happen to do so. Figure 2(b) indicates that in the small attraction limit the attraction does not act as a perturbation [36–40] in the presence of shear. As will be shown, the attraction always induces multiple types of solidlike states far below the jamming threshold and qualitatively alters the jamming phase diagram for purely repulsive particles.

Systems at $\phi > \phi_{j,\mu}$ are essentially jammed without the need of shear, which does not interest us here. The focus of this work is on the regime of $\phi < \phi_{j,\mu}$, where direct quenching always finds unjammed states and solidlike states can be explored with the help of shear. In the following, we will mainly discuss shear-driven solids at $\phi < \phi_{j,\mu}$. Results for $\phi > \phi_{j,\mu}$ are presented just for comparison.

C. "Time step" issue of the minimization and protocol dependence

The FIRE method that we use to find solid-like states is based on molecular dynamics simulation, which involves a tunable "time step" δt [30]. Because the strength of attraction μ that we study is so small, the preset δt has to be small enough to ensure small enough step increases of shear strain. Large step increases of shear strain induced by a large preset δt will break bonds and lead to the failure of finding shear-driven solids. As shown in Fig. 3(a), at fixed packing fraction, the probability of finding shear-driven solids $P(\sigma)$ under applied shear stress σ increases with decreasing the initial input value of δt as expected and becomes saturate when δt is small enough. We always use small enough δt when calculating $P(\sigma)$.

It has been known that the critical packing fraction ϕ_j of the jamming transition for purely repulsive particles depends on protocols [5,18–22]. For instance, ϕ_j could vary with the rate of compression and initial states. A relatively unbiased way to locate ϕ_j is to quickly quench ideal gas states to local potential energy minima and calculate the probability of finding jammed states at fixed packing fraction, as discussed in Ref. [5] and in Fig. 1(a). This protocol unbiasedly samples the inherent structures [19], which do not encounter the compression rate or route dependence.

In this work, we employ the same protocol to sample shear-driven solids at fixed packing fraction ϕ and shear stress σ, by minimizing the thermodynamiclike potential H. We estimate the probability of finding shear-driven solids $P(\sigma)$ and determine the yield stress from it. Therefore, each data point on the yield stress curve $\sigma_y(\phi)$ shown in Fig. 2(b) results from the direct sampling of the configurational space under the constraint of constant packing fraction and shear stress. It has nothing to do with the route approaching yielding, e.g., along constant packing fraction or along constant shear stress.

We have to acknowledge that, if we approach the yield stress by successively compressing (decompressing) states at fixed shear stress or decreasing (increasing) shear stress at fixed packing fraction, the yield stress may show route dependence. This route dependence should be a quite interesting issue to attack, which is out of the scope of current study. We hope to investigate it in detail in follow-up studies. The presence of attraction may lead to more complicated protocol dependence than purely repulsive systems. As demonstrated in Fig. 3(b), under quasistatic shear, an initially unjammed state with attraction evolves into solidlike states when the shear strain γ is greater than the threshold value γ_c. When we quasistatically shear the system backwards, the system cannot return to the unjammed state, but remains rigid. This hysteresis results from the presence of attraction and implies the possible complexity of the protocol dependence, which has also been observed in the same system under compression and decompression [12].

D. Shear stress and packing fraction dependence

Figures 4(a)–4(f) are configurations with force network of shear-driven solids at different packing fractions and shear stresses. At $\phi \ll \phi_{j,\mu}$, attraction (red bonds) dominates and the states look gel-like with fractal structures. Slightly above $\phi_{j,\mu}$, the structure looks uniform and particle interactions are predominantly repulsive (blue bonds). In between, with

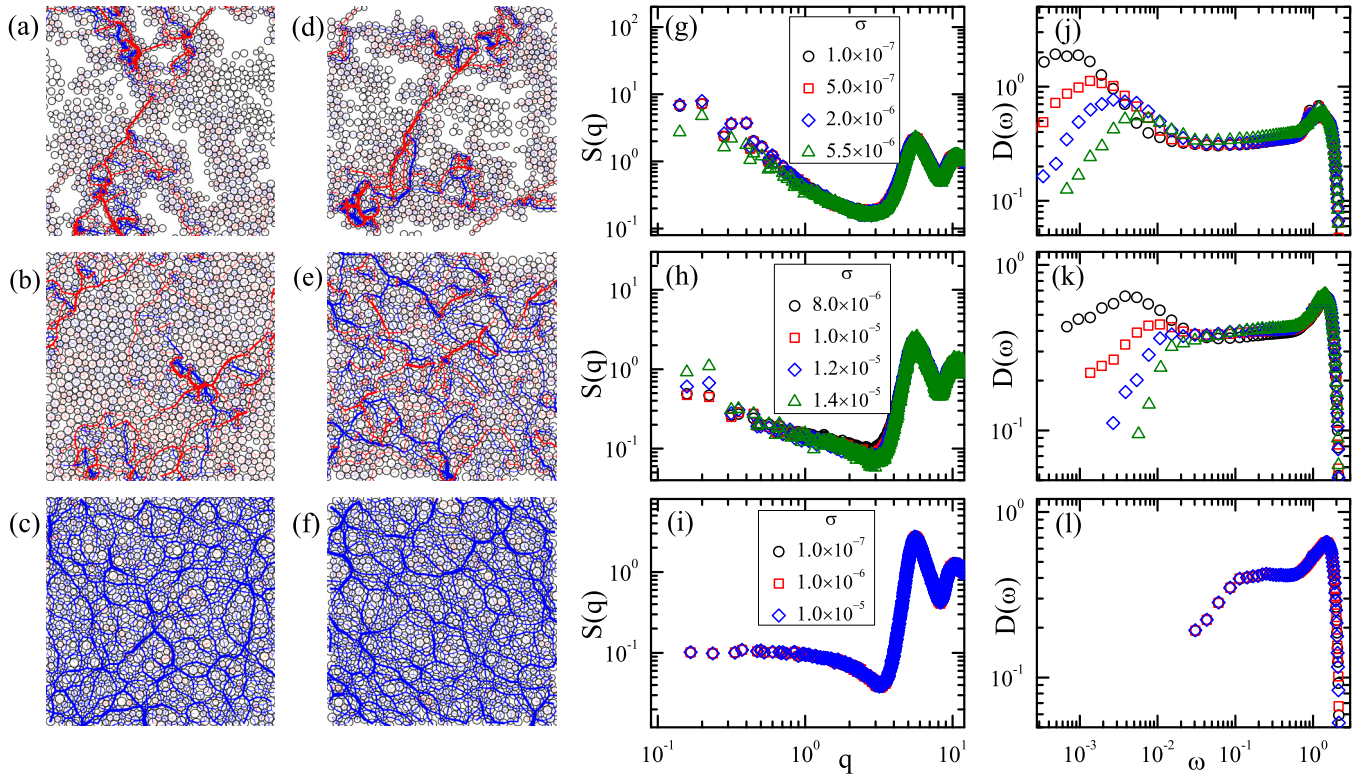

FIG. 4. (a)–(f) Snapshots, (g)–(i) static structure factor $S(q)$, and (j)–(l) DOVS $D(\omega)$ for solidlike states ($\mu = 10^{-3}$) driven by different shear stresses and at different packing fractions: $\phi = 0.60$ (top row), 0.75 (middle row), and 0.84 (bottom row). For (a)–(c), $\sigma = 10^{-6}$ (well below the yield stress), while for (d)–(f) $\sigma = 6 \times 10^{-6}$, 2×10^{-5}, and 2×10^{-4}, respectively, which are all near the yield stress. The red (blue) lines in (a)–(f) are attractive (repulsive) interactions, with the thickness illustrating the strength. To have a better vision, we normalize the interaction strength by the maximum value for every snapshot. The shear stress values of the $D(\omega)$ curves are listed in the legend of the $S(q)$ panels to the left.

increasing packing fraction, the structure evolves from gel-like to jamminglike.

Figures 4(g)–4(i) demonstrate the packing fraction and shear stress evolution of the static structure factor $S(q)$. The structure is almost independent of shear stress, while it evolves strongly with packing fraction. At $\phi \ll \phi_{j,\mu}$, the low q part of $S(q)$ exhibits the typical gel-like feature $S(q) \sim q^{-d_f}$ with $d_f \leqslant 2$ being the fractal dimension [41]. The low q part of $S(q)$ moves down with increasing packing fraction, and eventually becomes flat (jamminglike feature [42–44]) near $\phi_{j,\mu}$.

Purely from the packing fraction evolution of $S(q)$, we cannot determine the boundary between gel-like and glass or jamminglike states. Note that the solidlike states are shear induced. Although the structure is insensitive to the change of shear stress, other quantities may exhibit shear stress dependence and provide useful information to distinguish states. Comparing states at the same packing fraction but different shear stresses [e.g., Figs. 4(b) and 4(e)], we can tell that the shear stress indeed remarkably affects the force network: More particles interact and repulsion plays a more important role with increasing shear stress.

Resulting from significant changes in the force network, vibrational properties of shear-driven solids exhibit strong shear stress dependence. Figures 4(j)–4(l) show the shear stress evolution of the DOVS, $D(\omega)$. When $\phi > \phi_{j,\mu}$, applying shear stress only weakly affects the force network and elastic properties [23,24]. As shown in Fig. 4(l), $D(\omega)$ at different shear stresses overlap. Interestingly, Figs. 4(j) and 4(k) show that $D(\omega)$ has strong shear stress dependence when $\phi < \phi_{j,\mu}$. For solidlike states induced by small shear stresses, there is a low-frequency peak in $D(\omega)$, indicating the aggregation of soft modes. With increasing shear stress, the peak moves down and to higher frequencies, implying the decrease of the amount of soft modes and that shear-driven solids become stiffer and more stable.

At all packing fractions below $\phi_{j,\mu}$, the motion of the low-frequency peak in $D(\omega)$ with the change of shear stress follows the same trend. However, at low packing fractions where shear-driven solids are typically gel-like, until at the yield stress, the peak is still present. In contrast, near $\phi_{j,\mu}$, the peak disappears at a crossover shear stress $\sigma_c < \sigma_y$. Meanwhile, $D(\omega)$ exhibits a plateau, which is actually one of the most representative features of marginally jammed solids of purely repulsive particles [25–27,45]. When $\sigma > \sigma_c$, the evolution of $D(\omega)$ looks like that of marginally jammed solids under compression, but here the shear stress is the driving force instead of the packing fraction.

For marginally jammed solids, the flattening of $D(\omega)$ is associated with isostaticity [25–27,45], i.e., the average coordination number $z = z_c = 2d$ with d being the dimension of space. Is the emergence of the plateau in $D(\omega)$ at σ_c also related to isostaticity?

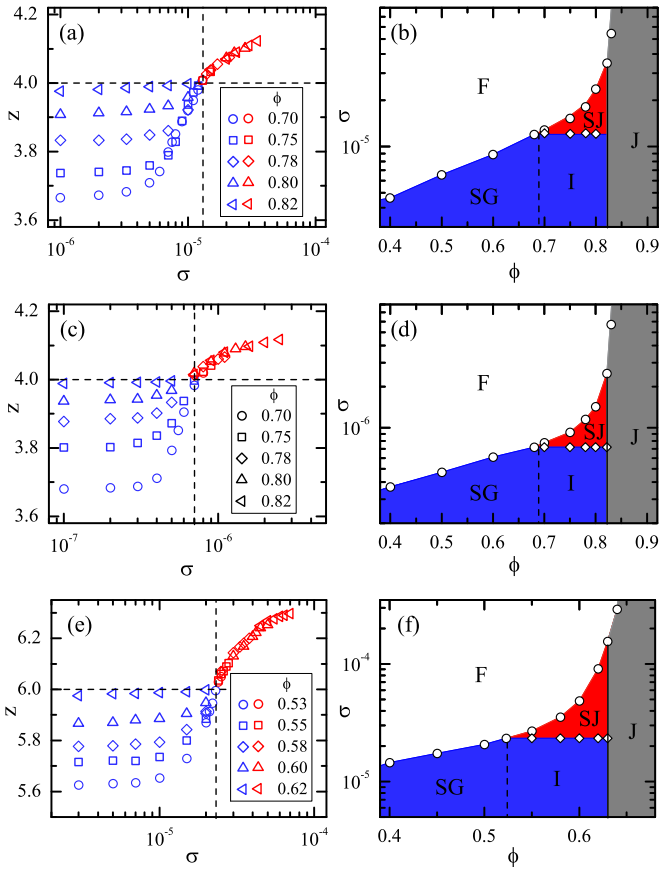

FIG. 5. Left column: Shear stress dependence of the average coordination number $z(\sigma)$ for shear-driven solids ($\mu = 10^{-3}$) at $\phi < \phi_{j,\mu}$. At each packing fraction, the blue (red) symbols denote data below (above) the crossover shear stress σ_c and with (without) low-frequency peak in the DOVS. The horizontal and vertical dashed lines label $z = z_c$ and $\sigma = \sigma_c$. Right column: Jamming phase diagram for weakly attractive particles ($\mu = 10^{-3}$) at $T = 0$. The circles and diamonds are the yield stress $\sigma_y(\phi)$ and crossover shear stress $\sigma_c(\phi)$, respectively. The solid and dashed vertical lines are $\phi = \phi_{j,\mu}$ and $\phi = \phi_{rp}$. F, SJ, SG, I, and J denote regimes of flowing (white), shear jammed (red), shear gel like (blue, $\phi < \phi_{rp}$), intermediate (blue, $\phi_{rp} < \phi < \phi_{j,\mu}$), and jammed (gray, $\phi > \phi_{j,\mu}$) states, respectively. The top, middle, and bottom panels are for two-dimensional harmonic ($z_c = 4$, $\sigma_c \approx 1.2 \times 10^{-5}$), two-dimensional Hertzian ($z_c = 4$, $\sigma_c \approx 7.1 \times 10^{-7}$), and three-dimensional harmonic systems ($z_c = 6$, $\sigma_c \approx 2.3 \times 10^{-5}$), respectively, all with $N = 1024$. Note that the rigidity percolation packing fraction is $\phi_{rp} \approx 0.524$ in three dimensions.

E. Isostaticity and strictly defined shear jamming

Figure 5(a) shows the shear stress evolution of the average coordination number (rattlers excluded) at $\phi < \phi_{j,\mu}$. When the shear stress is small, there is a plateau in $z(\sigma)$. The plateau value approaches z_c from below with increasing packing fraction. Approaching the yield stress, the coordination number grows quickly and collapses onto a master curve. In each $z(\sigma)$ curve, data points at $\sigma < \sigma_c$ and with the low-frequency peak in $D(\omega)$ are denoted by blue symbols, while red symbols represent data at $\sigma > \sigma_c$. Surprisingly, $z = z_c = 4$ is exactly the boundary between two colors, indicating that isostaticity is indeed coupled to the flattening of $D(\omega)$ at σ_c. Moreover, the collapse of all data at $z > z_c$ implies that the value of σ_c is independent of the packing fraction.

Now we see that solidlike states driven by a shear stress greater than σ_c possess important features of marginally jammed solids, such as $z > z_c$ and jamminglike $D(\omega)$. It is thus plausible to strictly define them as shear jammed solids. The transition into shear jamming is driven by the shear stress, which resembles the jamming transition of frictionless and purely repulsive particles driven by the packing fraction, but now a critical-like point at ϕ_j is replaced by a range of packing fractions.

F. Jamming phase diagram

Our major findings lead to the jamming phase diagram for weakly attractive particles in the σ-ϕ plane at $T = 0$. Figure 5(b) is an example of the diagram for $\mu = 10^{-3}$.

Strictly defined shear jamming (SJ) is encircled by $\phi = \phi_{j,\mu}$, $\sigma_y(\phi)$, and $\sigma = \sigma_c$. Interestingly, $\sigma = \sigma_c$ intersects $\sigma_y(\phi)$ roughly at the rigidity percolation threshold ϕ_{rp}. As mentioned earlier, solely from $S(q)$, it is hard to determine the crossover packing fraction to separate gel like states from jamminglike states. Now that SJ states only exist at $\phi > \phi_{rp}$, together with the evidence shown in Fig. 2(b), $\phi = \phi_{rp}$ is a plausible candidate of such a crossover.

Shear-driven solids lying below $\sigma = \sigma_c$ share some common features, e.g., existence of the low-frequency peak in $D(\omega)$, $z < z_c$, and attraction dominant, although they cover a wide range of packing fractions and exhibit progressive packing fraction evolution of the structure. States between ϕ_{rp} and $\phi_{j,\mu}$ are particularly interesting. They have similar structures to shear jammed states but resemble shear gel like states at $\phi < \phi_{rp}$ in mechanical and vibrational properties. We tentatively name them as intermediate states. The existence of intermediate states can only be found by the careful study of the shear stress dependence. It also warns us about the danger to identify various types of amorphous solids from structure [41] or vibrational properties [46] alone.

In order to verify that our major findings are not limited to specific potential and to two dimensions, in Figs. 5(c)–5(f), we show $z(\sigma)$ and the jamming phase diagram for two-dimensional Hertzian systems and for three-dimensional harmonic systems, respectively. Our major findings hold for all these systems.

G. Finite size effects

One may wonder if the existence of the SJ region discussed with the jamming phase diagram is a finite size effect. For purely repulsive particles, previous studies have shown that small size systems can jam below the critical packing fraction ϕ_j of the jamming transition. However, as an example shown in Fig. 1(a), the probability of finding jammed states in the absence of shear with $\mu = 10^{-3}$ is statistically zero when $\phi < 0.81$, while SJ states still survive below $\phi = 0.70$. Therefore, attraction and shear stress are both essential to the formation of SJ states, which is not simply due to finite size effects discussed above.

It has been shown that the yield stress of jammed solids of purely repulsive particles decreases with increasing system

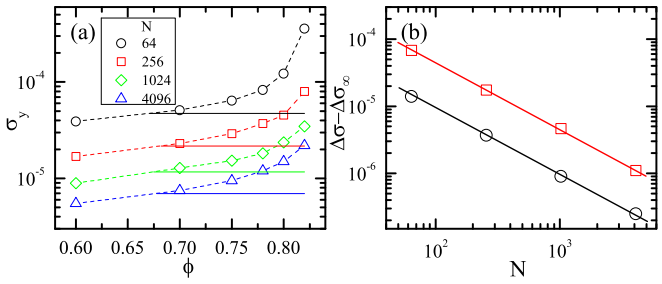

FIG. 6. (a) System size dependence of the yield stress $\sigma_y(\phi)$ for harmonic particles with $\mu = 10^{-3}$ in two dimensions. The horizontal solid lines label the crossover shear stress σ_c. The dashed lines are a guide for the eye. (b) System size scaling of $\Delta\sigma = \sigma_y - \sigma_c$, i.e., the shear stress gap between the yield stress σ_y and σ_c in which SJ states exist, at $\phi = 0.75$ (circles) and 0.80 (squares). The solid lines are power-law scaling fits to the data: $\Delta\sigma - \Delta\sigma_\infty \sim N^{-1}$, where $\Delta\sigma_\infty = 2.26 \times 10^{-6}$ (6.90×10^{-6}) for $\phi = 0.75$ (0.80).

size and approaches a limiting value in the large system size limit [23,24,43]. Figure 6(a) shows that the yield stress of shear-driven solids with attraction also decreases with increasing system size. For all system sizes studied, we find that the crossover shear stress σ_c at which shear-driven solids are isostatic and have a flattened density of vibrational states is constant in packing fraction. With increasing system size, σ_c decreases as well, but $\sigma_c(\phi)$ and $\sigma_y(\phi)$ always intersect approximately at $\phi = \phi_{rp} \approx 0.689$, so the density interval for SJ states to exist seems almost insensitive to the change of system size. In Fig. 6(b), we show the system size dependence of $\Delta\sigma = \sigma_y - \sigma_c$ for SJ states at two different packing fractions. $\Delta\sigma$ at both packing fractions can be well fitted with the same power-law scaling: $\Delta\sigma - \Delta\sigma_\infty \sim N^{-1}$, where $\Delta\sigma_\infty$ is the extrapolation in the $N \to \infty$ limit. At both packing fractions, $\Delta\sigma_\infty > 0$. Therefore, our results suggest that SJ regime does not vanish in large systems.

IV. DISCUSSION AND CONCLUSIONS

In summary, in the presence of weak attraction, athermal solidlike states are explored by shear over a wide range of packing fractions below the jamming transition. Our careful study of the packing fraction and shear stress dependence reveals that the static structure of shear-driven solids is sensitive to the change of packing fraction, but not to shear stress. In contrast, the DOVS and force network evolve unexpectedly and progressively with shear stress. The strong shear stress dependence enables us to determine strictly defined shear jamming and construct a jamming phase diagram in the σ-ϕ plane.

As shear stress increases, the rigidity of shear-driven solids at $\phi < \phi_{j,\mu}$ increases, reflected in the decay of soft modes and increase of the coordination number and elastic moduli (not shown). In contrast, increasing shear stress slightly softens jammed solids well above $\phi_{j,\mu}$. This opposite behavior on both sides of $\phi_{j,\mu}$ is analogous to that of thermal systems: With increasing temperature, glasses are hardened below the jamminglike transition, while slightly softened above [47,48]. Therefore, we provide evidence supporting that the shear stress can have similar effects as the temperature on transitions between liquidlike and solidlike states and properties of amorphous solids [49,50], as proposed by the original jamming phase diagram [1].

Our work is relevant to experimental systems like granular materials and non-Brownian colloids. For colloidal systems with Brownian motion, how temperature affects shear-induced solidification is interesting to attack next. Both the thermal motion and shear can harden systems at $\phi < \phi_{j,\mu}$. It is quite interesting to figure out whether and how they may compete or help each other to induce unpredictable results in dynamics and phase behaviors.

ACKNOWLEDGMENTS

We are grateful to K. Chen and J. Zhang for helpful discussions. This work was supported by National Natural Science Foundation of China Grants No. 21325418 and No. 11574278, National Basic Research Program of China (973 Program) Grant No. 2012CB821500, and Fundamental Research Funds for the Central Universities Grants No. 2030020028 and No. 2030020023. We also thank the Supercomputing Center of University of Science and Technology of China for computer time.

[1] A. J. Liu and S. R. Nagel, Nature (London) **396**, 21 (1998).
[2] A. J. Liu and S. R. Nagel, Annu. Rev. Condens. Matter Phys. **1**, 347 (2010).
[3] V. Trappe, V. Prasad, L. Cipelletti, P. N. Segre, and D. A. Weitz, Nature (London) **411**, 772 (2001).
[4] M. van Hecke, J. Phys.: Condens. Matter **22**, 033101 (2010).
[5] C. S. O'Hern, L. E. Silbert, A. J. Liu, and S. R. Nagel, Phys. Rev. E **68**, 011306 (2003).
[6] G. Parisi and F. Zamponi, Rev. Mod. Phys. **82**, 789 (2010).
[7] P. J. Lu, E. Zaccarelli, F. Ciulla, A. B. Schofield, F. Sciortino, and D. A. Weitz, Nature (London) **453**, 499 (2008).
[8] P. J. Lu and D. A. Weitz, Annu. Rev. Condens. Matter Phys. **4**, 217 (2013).
[9] W. C. K. Poon and M. D. Haw, Adv. Colloid Interface **73**, 71 (1997).
[10] E. Zaccarelli, J. Phys.: Condens. Matter **19**, 323101 (2007).
[11] D. Bi, J. Zhang, B. Chakraborty, and R. P. Behringer, Nature (London) **480**, 355 (2011).
[12] G. Lois, J. Blawzdziewicz, and C. S. O'Hern, Phys. Rev. Lett. **100**, 028001 (2008).
[13] C. Song, P. Wang, and H. A. Makse, Nature (London) **453**, 629 (2008).
[14] A. Donev, I. Cisse, D. Sachs, E. Variano, F. H. Stillinger, R. Connelly, S. Torquato, and P. M. Chaikin, Science **303**, 990 (2004).
[15] P. F. Damasceno, M. Engel, and S. C. Glotzer, Science **337**, 453 (2012).

[16] S. Torquato and Y. Jiao, Nature (London) **460**, 876 (2009).
[17] C. F. Schreck, N. Xu, and C. S. O'Hern, Soft Matter **6**, 2960 (2010).
[18] S. Torquato, T. M. Truskett, and P. G. Debenedetti, Phys. Rev. Lett. **84**, 2064 (2000).
[19] N. Xu, J. Blawzdziewicz, and C. S. O'Hern, Phys. Rev. E **71**, 061306 (2005).
[20] P. Chaudhuri, L. Berthier, and S. Sastry, Phys. Rev. Lett. **104**, 165701 (2010).
[21] M. Ozawa, T. Kuroiwa, A. Ikeda, and K. Miyazaki, Phys. Rev. Lett. **109**, 205701 (2012).
[22] L. Berthier, D. Coslovich, A. Ninarello, and M. Ozawa, Phys. Rev. Lett. **116**, 238002 (2016).
[23] H. Liu, H. Tong, and N. Xu, Chin. Phys. B **23**, 116105 (2014).
[24] H. Liu, X. Xie, and N. Xu, Phys. Rev. Lett. **112**, 145502 (2014).
[25] L. E. Silbert, A. J. Liu, and S. R. Nagel, Phys. Rev. Lett. **95**, 098301 (2005).
[26] M. Wyart, S. R. Nagel, and T. A. Witten, Europhys. Lett. **72**, 486 (2005).
[27] M. Wyart, L. E. Silbert, S. R. Nagel, and T. A. Witten, Phys. Rev. E **72**, 051306 (2005).
[28] E. Irani, P. Chaudhuri, and C. Heussinger, Phys. Rev. Lett. **112**, 188303 (2014).
[29] M. P. Allen and D. J. Tildesley, *Computer Simulation of Liquids* (Oxford University Press, New York, 1987).
[30] E. Bitzek, P. Koskinen, F. Gahler, M. Moseler, and P. Gumbsch, Phys. Rev. Lett. **97**, 170201 (2006).
[31] http://www.caam.rice.edu/software/ARPACK.
[32] E. Somfai, M. van Hecke, W. G. Ellenbroek, K. Shundyak, and W. van Saarloos, Phys. Rev. E **75**, 020301 (2007).
[33] H. A. Vinutha and S. Sastry, Nat. Phys. **12**, 578 (2016).
[34] S. Sarkar, D. Bi, J. Zhang, J. Ren, R. P. Behringer, and B. Chakraborty, Phys. Rev. E **93**, 042901 (2016).
[35] N. Xu and C. S. O'Hern, Phys. Rev. E **73**, 061303 (2006).
[36] L. Berthier and G. Tarjus, Phys. Rev. Lett. **103**, 170601 (2009).
[37] L. Berthier and G. Tarjus, Phys. Rev. E **82**, 031502 (2010).
[38] L. Berthier and G. Tarjus, J. Chem. Phys. **134**, 214503 (2011).
[39] Z. Zhang, P. J. Yunker, P. Habdas, and A. G. Yodh, Phys. Rev. Lett. **107**, 208303 (2011).
[40] L. Wang and N. Xu, Phys. Rev. Lett. **112**, 055701 (2014).
[41] H. Tanaka, J. Meunier, and D. Bonn, Phys. Rev. E **69**, 031404 (2004).
[42] A. Donev, F. H. Stillinger, and S. Torquato, Phys. Rev. Lett. **95**, 090604 (2005).
[43] N. Xu and E. S. C. Ching, Soft Matter **6**, 2944 (2010).
[44] L. Berthier, P. Chaudhuri, C. Coulais, O. Dauchot, and P. Sollich, Phys. Rev. Lett. **106**, 120601 (2011).
[45] L. Wang and N. Xu, Soft Matter **9**, 2475 (2013).
[46] M. A. Lohr, T. Still, R. Ganti, M. D. Gratale, Z. S. Davidson, K. B. Aptowicz, C. P. Goodrich, D. M. Sussman, and A. G. Yodh, Phys. Rev. E **90**, 062305 (2014).
[47] X. Wang, W. Zheng, L. Wang, and N. Xu, Phys. Rev. Lett. **114**, 035502 (2015).
[48] A. Ikeda, L. Berthier, and P. Sollich, Phys. Rev. Lett. **109**, 018301 (2012).
[49] H. N. Lee, K. Paeng, S. F. Swallen, and M. D. Ediger, Science **323**, 231 (2009).
[50] D. A. Weitz, Science **323**, 214 (2009).